Journal of Applied Mechanics and Technical Physics, Vol. 38, No. 5, 1997

ESTIMATION OF THE CARRYING CAPACITY OF CONICAL ACRYLIC WINDOWS

V. P. Lyanzberg and V. I. Shalashilin

UDC 539.3.621.12.001.2

A window with a light-transmitting glass element of organic glass is often designed by the scheme shown in Fig. 1. Under the action of pressure P, the conical element 1 is shifted over the conical surface of the casing 2 to the position shown by the dotted curve in Fig. 1. Experimental studies of such windows are described in [1, 2], which report the results of the first two series of tests with a cone angle $\alpha = 60°$.

In the next two series of experiments, glass elements with $\alpha = 30$, 45, and 90° were studied. The diameter of the large base of all glass elements is $94 \cdot 10^{-3}$ m, and the ratio of its thickness h to the smaller diameter d for each value of α is equal to $\delta = 0.1$, 0.3, and 0.5. The acute angle between the lateral surface and the large base was not rounded off ($r = 2 \cdot 10^{-3}$ m). The angle between the smaller base and the lateral surface was not rounded off. The bases were polished to transparency. The glass elements were made of block organic glass that was used for specimens of the first two series. In the casings, made of 30KhGSA steel, the height of the conical cavity h_1 exceeded the thickness of the glass element by $(10–15) \cdot 10^{-3}$ m. In this case, the glass element was located in the conical cavity of the casing up to complete failure. The casing and the glass element were fitted to one another. There was no intermediate layer. In the initial step of loading, sealing was performed by applying a hermetic layer on the edge of the large base.

Analysis of the results of all experiments leads to the following conclusions.

By failure characteristics and the type of dependence of the axial displacement of the lower base w on the hydrostatic pressure P, we can distinguish windows with $\alpha = 90°$ and $\delta = 0.1$ (thin specimens). They fail by splitting into sectors. The curve of $P(w)$ has two characteristic sections: initial and nonlinear. Apparently, failure of such specimens is a result of bending.

As δ increases, the character of failure and the shape of the curve of $P(w)$ change qualitatively. Thus, for example, failure of specimens with $\alpha = 90°$ and $\delta = 0.3$ begins with cleavage of the cone-shaped segment on the unloaded base. The larger (loaded) base remains plane. As the cone angle of the window decreases with fixed value of δ, the cone-shaped segment cleaved in the first step of failure increases. A similar dependence is observed for specimens at constant value of α with increase in δ.

With elevation and drop of pressure for specimens with $\alpha = 30$ and 45°, the curve of $P(w)$ has the shape of a hysteresis loop. The glass elements do not return to the initial state. The smaller the cone angle, the larger the residual displacement of the glass element. It also increases with increase in pressure.

The experiments revealed a number of peculiarities in the behavior of glass elements with $\delta > 0.1$. The first of these is that the fracturing pressure depends significantly on the friction coefficient on the surface contact between the glass element and the casing. In tests, various friction coefficients are obtained by using various intermediate layers between glass elements and casings. At the same time, the radial strain ε_r on the lower surface of the glass element remains stable at the moment of failure. It is considerably smaller than the failure strain ε_b for organic glass.

For the small friction coefficient, the failure pressure decreases, because, in this case, the axial displacement of the lower base of the glass element reaches a limiting value at lower external pressure.

For $\alpha = 30°$ and $\delta > 0.14$, and a small friction coefficient, the failure character changes qualitatively: under axisymmetric loading it becomes nonaxisymmetric.

Moscow Aviation Institute, Moscow 125871. Translated from Prikladnaya Mekhanika i Tekhnicheskaya Fizika, Vol. 38, No. 5, pp. 173–180, September–October, 1997. Original article submitted December 18, 1995; revision submitted April 1, 1996.

0021-8944/97/3805-0807 $18.00

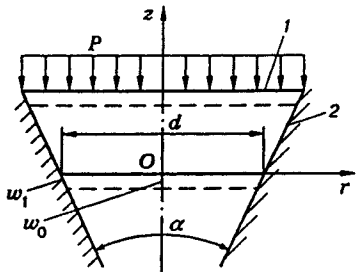

Fig. 1

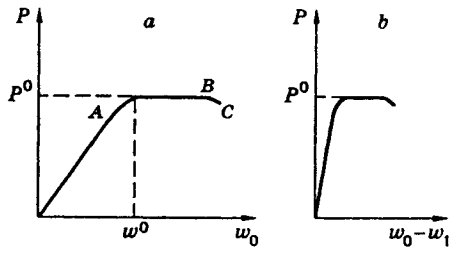

Fig. 2

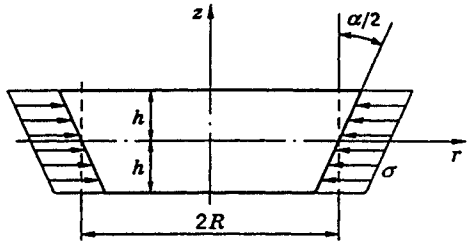

Fig. 3

For loading and unloading of specimens with $\alpha = 30$ and 45°, the residual displacement of the glass element decreases as the friction coefficient decreases. These results confirm the conclusion drawn in [1, 2]: the presence of a loop of the hysteresis type is related to the slippage of specimens in the conical cavity of the casing.

The second feature is the type of dependence of deflection of the point O of the glass element w_0 on the pressure, which is shown in Fig. 2a. The presence of the section AB, and, in particular, of the descending section BC, cannot be explained by the type of the σ–ε diagram of the material, because, under compression, it increases monotonically up to the moment of failure because of the formation of an antineck.

These features suggest that the loss of stability of the material near its lower surface is responsible for the failure of the glass element. This still further underlines the dependence of P on $w_0 - w_1$ (Fig. 2b), where w_0 is the displacement of the glass element at the center, and w_1 is the displacement near the casing. It becomes clear that the failure is preceded by buckling at the center of the glass element.

To evaluate critical stresses, we consider the stability problem for a conical element that is uniformly compressed by radial stresses (Fig. 3). The solution is constructed on the basis of the equations of the linearized three-dimensional theory of stability [3] obtained under the assumption that the subcritical stress–strain state is uniform. These equations are written in tensor form:

$$L_{m\alpha}u_\alpha = 0, \quad L_{m\alpha} = \omega_{im\alpha\beta}\frac{\partial^2}{\partial x_i \partial x_\beta}, \quad i, m, \alpha, \beta = 1, 2, 3, \tag{1}$$

where u_i is the displacement in the x_i direction. Values of the coefficients $\omega_{im\alpha\beta}$ are given in [3]. We restrict ourselves to axisymmetric deformation and denote $x_1 = r$ and $x_2 = z$. The end surfaces of the elements ($z = \pm h$) are considered free of stresses $\sigma_{zz} = 0$ and $\tau_{rz} = 0$.

We assume that, on the lateral conical surface of the elements, the conditions

$$u_r = 0, \quad \partial u_z/\partial r = 0, \quad r = R + \beta z, \quad \beta = \tan(\alpha/2)$$

hold. This corresponds to rigid clamping of the lateral surface.

After introduction of the resolving function χ, system (1) reduces to the equation

$$\left(\Delta + \Omega \frac{\partial^2}{\partial z^2}\right)\left(\Delta + (\Omega + A)\frac{\partial^2}{\partial z^2}\right)\chi = 0. \tag{2}$$

Here

$$\Omega = \frac{1}{1 + \sigma^0/\mu}; \qquad \Omega + A = \frac{1}{1 + \sigma^0/(\lambda + 2\mu)},$$

where λ and μ are Lamé constants, σ^0 are the desired critical stresses, and Δ is the Laplacian.

The boundary conditions take the following form:
on the lateral surface,

$$\frac{\partial^2}{\partial r \partial z}\chi\Big|_{r=R+\beta z} = 0, \quad \left(\Delta \frac{\partial}{\partial r}\chi + (\Omega + B)\frac{\partial^2}{\partial r \partial z}\chi\right)\Big|_{r=R+\beta z} = 0, \quad B = \frac{\mu}{\sigma^0 + \lambda + 2\mu}; \tag{3}$$

and on the end surface ($z = \pm h$),

$$\begin{gathered}\left[1 - \frac{\lambda(\lambda+\mu)}{(\lambda+2\mu)^2}(\Omega + A)\right]\frac{\partial}{\partial z}\Delta\chi + \frac{\mu}{\lambda+2\mu}(\Omega + A)\frac{\partial^3}{\partial z^3}\chi = 0, \\ \frac{\partial}{\partial r}\Delta\chi - (\Omega + A)\frac{\lambda}{\lambda+2\mu}\frac{\partial^3}{\partial r \partial z^2}\chi = 0.\end{gathered} \tag{4}$$

The boundary-value problem (3) and (4) will be solved by the method of perturbation of the boundary of a region (see [4, Sec. 5.5]). This method, in contrast to the traditional perturbation method [5], does not require transformation to a special coordinate system in which the conical element occupies a canonical region. This simplifies the manipulations significantly.

The conical element will be considered as a perturbation of the cylindrical element shown in Fig. 3 by a dashed curve. As the perturbation parameter, we use $\beta = \tan(\alpha/2)$. According to the methodical procedure, we represent the function $\chi(r, z, \beta)$ and the parameters Ω and $\Omega + A$ as power series in β:

$$\begin{gathered}\chi = \chi^{(0)} + \frac{\beta^2}{2!}\chi^{(2)} + \frac{\beta^4}{4!}\chi^{(4)} + \dots, \quad \Omega = \Omega^{(0)} + \frac{\beta^2}{2!}\Omega^{(2)} + \frac{\beta^4}{4!}\Omega^{(4)} + \dots, \\ \Omega + A = (\Omega^{(0)} + A) + \frac{\beta^2}{2!}\Omega^{(2)} + \frac{\beta^4}{4!}\Omega^{(4)} + \dots .\end{gathered} \tag{5}$$

Here we take into account that the plane $z = 0$ is the middle (along the z axis) plane of the truncated cone. Problem (2)–(4) (Fig. 3) is even for β. Therefore, uneven powers for β are not taken into account.

On the lateral surface, $r = R + \beta z$, and, hence, here $\chi(r, z, \beta) = \chi(\beta z + R, z, \beta)$. With allowance for this circumstance, the first series (5) on the lateral surface can be written as

$$\chi(\beta z + R, z, \beta) = \chi^{(0)} + \frac{\beta^2}{2!}\chi^{(2)} + \dots,$$

$$\chi^{(n)} = \frac{d^n}{d\beta^n}\chi(r = \beta z + R, z, \beta)\Big|_{\beta=0} = \left(\frac{\partial}{\partial\beta} + \frac{\partial r}{\partial\beta}\frac{\partial}{\partial r}\right)^n \chi\Big|_{\beta=0} = \left(\frac{\partial}{\partial\beta} + \frac{\partial r}{\partial\beta}\frac{\partial}{\partial r}\right)^n \chi\Big|_{\beta=0}$$

$$= \left(\frac{\partial}{\partial\beta} + z\frac{\partial}{\partial r}\right)\chi(r, z, \beta)\Big|_{\beta=0} = \sum_{j=0}^{n} C_n^j z^j \frac{\partial^j}{\partial r^j}\chi^{(n-j)}\Big|_{\beta=0}, \quad C_n^j = \frac{n!}{j!(n-j)!}, \quad n = 2, 4 \dots .$$

We substitute the resulting expressions into Eq. (2) and into the boundary conditions (3) and (4) and group terms of equal powers of β. As a result, we obtain the following recursive sequence of boundary-value problems. [Below, the conditions at the ends ($z = \pm h$) are not given, because they coincide in form with conditions (4).]

The zero approximation is of the form

$$\left(\Delta + \Omega^{(0)}\frac{\partial^2}{\partial z^2}\right)\left(\Delta + (\Omega^{(0)} + A)\frac{\partial^2}{\partial z^2}\right)\chi^{(0)} = 0,$$

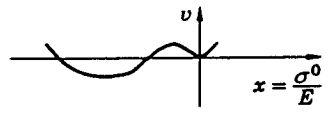

Fig. 4

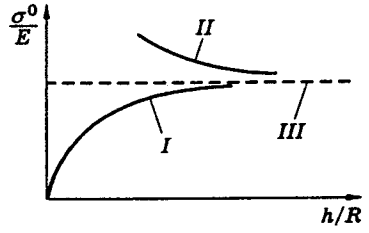

Fig. 5

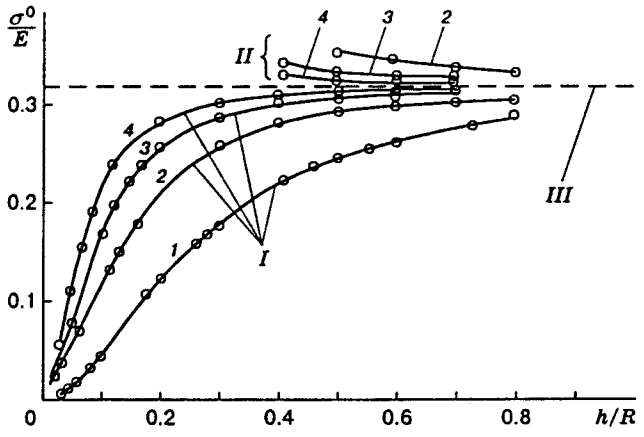

Fig. 6

$$\frac{\partial^2}{\partial r \partial z}\chi^{(0)}\Big|_{r=R} = 0, \quad \left(\Delta \frac{\partial}{\partial r}\chi + \beta \frac{\partial^3}{\partial r \partial z^2}\chi\right)\Big|_{r=R} = 0,$$

and the second approximation is of the form

$$\left(\Delta + \Omega^{(0)}\frac{\partial^2}{\partial z^2}\right)\left(\Delta + (\Omega^{(0)} + A)\frac{\partial^2}{\partial z^2}\right)\chi^{(2)} = -2\Omega^{(2)}\frac{\partial^2}{\partial z^2}\Delta\chi^{(0)} - \Omega^{(2)}[2\Omega^{(0)} + A]\frac{\partial^4}{\partial z^4}\chi^{(0)},$$

$$\frac{\partial^2}{\partial r \partial z}\chi^{(2)} = \left(-z^2\frac{\partial^4}{\partial r^3 \partial z}\chi^{(0)} - 2z\frac{\partial^3}{\partial r^3}\chi^{(0)}\right)\Big|_{r=R},$$

$$\left(\Delta\frac{\partial}{\partial r}\chi^{(2)} + B\frac{\partial^3}{\partial r \partial z^2}\chi^{(2)}\right)\Big|_{r=R} = -\left[z^2\Delta\frac{\partial^3}{\partial r^3}\chi^{(0)} + B\left(z^2\frac{\partial^5}{\partial z^2 \partial r^3}\chi^{(0)} + 2\frac{\partial^3}{\partial r^3}\chi^{(0)} + 4z\frac{\partial^4}{\partial r^3 \partial z}\chi^{(0)}\right)\right]\Big|_{r=R}.$$

The problem in a zero approximation is solved in [3]. We write it as

$$\chi^{(0)} = J(\delta r)\left[C_1 \exp\left(\delta z/\sqrt{\Omega^{(0)}}\right) + C_2 \exp\left(-\delta z/\sqrt{\Omega^{(0)}}\right)\right.$$
$$\left. + C_3 \exp\left(\delta z/\sqrt{\Omega^{(0)} + A}\right) + C_4 \exp\left(-\delta z/\sqrt{\Omega^{(0)} + A}\right)\right].$$

The conditions of rigid clamping lead to $\delta = æ_l/R$, where $æ_l$ is a root of the first-order Bessel function J_1.

From the condition of existence of a nontrivial solution of the system for determining $C_1, \ldots, C_4$, we arrive at the characteristic equation

$$v = \left[m_1^2 c^2 + l_1^2 f_1^2\right]\sinh 2k \sinh 2d_1 - 2f_1 m_1 c l_1[\cosh 2k \cosh 2d_1 - 1] = 0. \tag{6}$$

Here

$$c = K + \frac{M}{\Omega^{(0)}}; \quad f_1 = K + \frac{M}{\Omega^{(0)} + A}; \quad l_1 = -\frac{L}{\Omega^{(0)}} + \frac{S}{(\Omega^{(0)})^{3/2}}; \quad m_1 = \frac{L}{\Omega^{(0)} + A} + \frac{S}{(\Omega^{(0)} + A)^{3/2}};$$

$$d_1 = \frac{æ_l h}{R\sqrt{\Omega^{(0)}}}; \quad k = \frac{æ_l h}{R\sqrt{\Omega^{(0)} + A}}; \quad L = 1 - \frac{\lambda(\lambda + \mu)}{(\lambda + 2\mu)^2}(\Omega^{(0)} + A); \quad S = \frac{\mu}{\lambda + 2\mu}(\Omega^{(0)} + A);$$

$$M = (\Omega^{(0)} + A)\frac{\lambda}{\lambda + 2\mu}; \quad K = 1; \quad \Omega^{(0)} = \frac{1}{1 + \sigma^{(0)}/\mu}.$$

The transcendental equation (6) was solved numerically. The behavior of the left side v as a function of $x = \sigma^0/E$ is shown in Fig. 4. In the range of real values $x = 0$–0.35, Eq. (6) has three roots, one of which corresponds to $x = 0$. The nonzero root that is smaller in absolute value corresponds to the bending form of loss of stability, and the second to the loss of stability with the formation of an antineck. The behavior of these roots as a function of h/d is illustrated in Fig. 5, where curve I corresponds to the bending form, and

curve II corresponds to the formation of an antineck. With increase in h/d, both solutions approach the value σ^0 that corresponds to surface instability (curve III).

The solution was studied numerically for various values of $æ_l$. Note that when $æ_l$ is equal to the first root of the Bessel function J_1, the solution of Eq. (6) is only the bending form of loss of stability, and, for the next values of $æ_l$, the solution exhibits two forms of loss of stability.

The character of the solution as a function of the parameter $æ_l$ for $l = 1$, 2, 3, and 4 is shown in Fig. 6. Here the curve number corresponds to the value of l, and I–III correspond to the notation in Fig. 5.

Thus in the general case of a fixed root of the Bessel function J_1, there are two nonzero solutions of the characteristic equation that correspond to the bending form of the loss of stability σ_1^0 and the loss of stability with the formation of an antineck σ_2^0. Each of these values of σ corresponds to a value of the parameter Ω. We denote it by Ω_{lm}, where l is the root number of the Bessel function J_1, and $m = 1$ corresponds to the bending form of loss of stability and $m = 2$ corresponds to the antineck.

To each Ω_{lm} correspond definite coefficients C_1, C_2, C_3, and C_4 in the general solution of stability equations. We denote them by C_{1lm}, C_{2lm}, C_{3lm}, and C_{4lm}.

Then, the eigenfunction that corresponds to the eigenvalue of the parameter $\Omega_{lm}^{(0)}$ that is a solution of the zero-order approximation problem can be written as

$$\chi_{lm} = J\left(\frac{æ_l r}{R}\right)\left\{C_{1lm}\exp\left[\frac{æ_l r}{R\sqrt{\Omega_{lm}^{(0)}}}\right] + C_{2lm}\exp\left[-\frac{æ_l r}{R\sqrt{\Omega_{lm}^{(0)}}}\right]\right.$$
$$\left. + C_{3lm}\exp\left[\frac{æ_l r}{R\sqrt{\Omega_{lm}^{(0)} + A}}\right] + C_{4lm}\exp\left[-\frac{æ_l r}{R\sqrt{\Omega_{lm}^{(0)} + A}}\right]\right\}. \tag{7}$$

The solution of the subsequent nth approximation is sought as the sum $\chi_{lm}^{(n)} = F_{lm}^{(n)} + U_{lm}^{(n)}$. The function U_{lm} was chosen so that it satisfies inhomogeneous boundary conditions. Then, $F_{lm}^{(n)}$ is a solution of the problem for inhomogeneous equations with homogenous boundary conditions and is defined as

$$F_{lm}^{(n)} = \sum_i \sum_k f_{lmik}^{(n)} \chi_{ik}^{(0)}.$$

We substitute (7) into the corresponding equation and orthogonalize it to the solution of the homogenous boundary-value problem with weight $\rho(r) = r$. For $l = m$ and $i = k$, we obtain an equation for determining the eigenvalue of the subsequent nth approximation.

The solution of the second approximation is of the form

$$\chi_{lm}^{(2)} = \sum_i \sum_k f_{lmik}\chi^{(0)} - z^2 \frac{\partial^2}{\partial r^2}\chi_{lmik}^{(0)}\Big|_{r=R}.$$

After orthogonalization for $l = i$ and $m = k$, we have the equation

$$\Omega_{lm}^{(2)} \int_0^R \int_{-h}^h \left[(2\Omega_{lm}^{(0)} + A)\frac{\partial^4}{\partial z^4}\chi_{lm}^{(0)} + 2\frac{\partial^2}{\partial z^2}\Delta\chi_{lm}^{(0)}\right]\chi_{lm}^{(0)} r\, dr dz$$
$$= \int_0^R \int_{-h}^h \left\{\left[\Delta\Delta + (2\Omega_{lm}^{(0)} + A)\Delta\frac{\partial^2}{\partial z^2} + (\Omega_{lm}^{(0)} + A)\Omega_{lm}^{(0)}\frac{\partial^4}{\partial z^4}\right]\left(-z^2\frac{\partial^2}{\partial r^2}\chi_{lm}^{(0)}\Big|_{r=R}\right)\right\}\chi_{lm}\, r dr dz.$$

Calculating the eigenvalue of the second approximation $\Omega_{lm}^{(2)}$, we obtain $\Omega_{lm} = \Omega_{lm}^{(0)} + \Omega_{lm}^{(2)}\beta^2/2$. We determine the critical value of the axial displacement via the resulting parameter Ω.

It was noted above that the axial displacement of the lower base does not depend on the friction coefficient. From this it follows that the corresponding radial stresses at the moment of failure do not depend on it either. Therefore, comparison of theoretical and experimental results for the axial displacement is equivalent to comparison of radial stresses. We assume that the quantity w is the displacement of the end of the lower

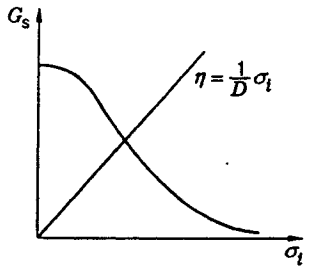

Fig. 7

TABLE 1

α, deg	$w^0 \cdot 10^{-3}$	$w_* \cdot 10^{-3}$	$w^0 \cdot 10^{-3}$	$w_* \cdot 10^{-3}$
	m			
	$\delta = 0.3$		$\delta = 0.5$	
30	4.9	5.2	5.78	6
45	3	3.4	3.4	3.7
60	2.01	2.4	2.6	3.1
90	1.3	1.8	1.9	—

base of the window. To w correspond the radial and circular strains

$$\varepsilon_r = \varepsilon_\theta = \frac{2w \tan(\alpha/2)}{d}$$

and the stresses

$$\sigma_r = \sigma_\theta = -\frac{E}{1-\nu^2} \frac{2w \tan(\alpha/2)}{d}.$$

Setting $\sigma_z = 0$, we find

$$\varepsilon_z = \frac{1}{E}[\sigma_z - \nu(\sigma_r - \sigma_\theta)] = \frac{2\nu}{1-\nu^2} \frac{2w \tan(\alpha/2)}{d}.$$

The strain intensity is given by the equation

$$\varepsilon_i = \frac{\sqrt{2}}{3}\sqrt{(\varepsilon_r - \varepsilon_\theta)^2 + (\varepsilon_\theta - \varepsilon_z)^2 + (\varepsilon_z - \varepsilon_r)^2} = \frac{4}{3}\frac{w \tan(\alpha/2)}{d}\left(1 - \frac{2\nu}{1-\nu^2}\right). \tag{8}$$

As the initial characteristic of the material, we used the σ–ε diagram, from which the strain diagram was constructed. For a two-axial stress state, we have

$$\sigma_i = \sigma, \qquad \varepsilon_i = \varepsilon - \varepsilon_\theta = \varepsilon - \frac{1-2\nu'}{3E}\sigma.$$

It follows from the experiments that, at the moment of failure of the window, the values of ε_i far exceed the strains at $\sigma_i = \sigma_{\text{proportional}}$.

The physically nonlinear behavior of the material was taken into account using the tangential-modulus concept. The dependence of G_s on σ_i for the given material was constructed from the σ_i–ε_i dependence by numerical integration (Fig. 7). Here G_s is the secant modulus.

The Poisson coefficient beyond the limit of proportionality ν' is given by the relation [6]

$$\nu' = \frac{1}{2} - \frac{1-2\nu}{2}\frac{E_s}{E},$$

where E_s is the secant modulus. Using the obtained value of Ω in the relation $\Omega = 1/(1 + \sigma^0/\mu)$, we obtain

$$\frac{\sigma}{G_s} = \left[\frac{1}{\Omega} + 1\right] = D.$$

In the $G_s - \sigma_i$ diagram (Fig. 7), the point of its intersection with the straight line $\eta = (1/D)\sigma_i$ gives the desired value of the critical stress σ^0.

The corresponding strain intensity was also found from the strain diagram. From relation (8), we also have the axial displacement

$$w^0 = \varepsilon_i \frac{3}{4}\cot\frac{\alpha}{2}\frac{1-\nu'^2}{1-\nu'^2-2\nu'}d.$$

The calculation and experimental results are given in Table 1. The following conclusion can be drawn. For $\alpha = 0$–$30°$, the values of the theoretical and experimental studies are close. With a further increase in α, the difference between the theoretical w^0 and experimental w_* critical values of the deflection increases. This is apparently due to the fact that, with increase in α, the stress state differs to a greater extent from the homogeneous state adopted in the calculations. Neither were the friction forces and the effect of bending taken into account.

The results suggest that the failure of windows, except for specimens with a small thickness-to-diameter ratio and a large value of α, is preceded by the loss of stability on the unloaded base of the conical element.

REFERENCES

1. J. D. Stachiw, "Critical pressure of conical acrylic windows under short-term hydrostatic loading," *J. Eng. Industry, Ser. B,* **89**, No. 3, 44–54 (1967).
2. V. P. Lyanzberg and V. I. Shalashilin, "Conical acrylic windows under short-term loading," *Probl. Prochn.*, No. 11, 106–111 (1983).
3. A. N. Guz', *Foundations of the Three-Dimensional Theory of Stability of Deformable Bodies* [in Russian], Vyshcha Shkola, Kiev (1986).
4. É. I. Grigolyuk and V. I. Shalashilin, *Problems of Nonlinear Deformation: Continuation Method in Nonlinear Problems of the Mechanics of Deformable Bodies* [in Russian], Nauka, Moscow (1988).
5. A. H. Nayfen, *Perturbation Methods*, John Wiley and Sons, New York–London–Sydney–Toronto (1973).
6. N. N. Malinin, *Applied Theory of Plasticity and Creep* [in Russian], Mashinostroenie, Moscow (1968).